



Electrochemical and theoretical studies of adsorption and corrosion inhibition of ethyl 5-amino-1-((8-hydroxyquinolin-5-yl) methyl)-1H-1,2,3-triazole-4-carboxylate on carbon steel in acidic solution

Z. Rouifi^{1,2}, M. El Faydy², H. About^{1,2}, F. Benhiba¹, H. Ramsis³, M. Boudalia⁴,
H. Zarrok¹, R. Tourir^{5,6}, M. El M'Rabet⁷, H. Oudda¹, A. Guenbour⁴, B. Lakhrissi²

¹Laboratoire des Procédés de Séparation, Faculté des Sciences, PO Box 242 Kenitra, Morocco

²Laboratoire d'Agroressources, Polymères et Génie des Procédés, Université Ibn Tofail, PO Box 242 Faculté des Sciences, Kenitra – Morocco

³Laboratoire de Spectroscopie, Département de Chimie, Faculté des sciences, Université Ibn Tofail, Kenitra, Morocco

⁴Dept. de Chimie, Laboratoire de Corrosion-Electrochimie, Faculté des Sciences de Rabat, Avenue Ibn Battouta, BP 1014 Rabat, Morocco.

⁵Laboratoire d'Ingénierie des Matériaux et d'Environnement : Modélisation et Application, Faculté des Sciences, Université Ibn Tofail, BP 133, Kenitra 14 000, Morocco.

⁶Centre Régional des Métiers de l'Éducation et de la Formation (CRMEF), Avenue Allal Al Fassi, Madinat Al Irfane BP 6210 Rabat, Morocco.

⁷Département DSFA, Unité de chimie, Institut Agronomique et Vétérinaire Hassan II. Rabat, Morocco.

Received 25 Apr 2017,
Revised 09 Sep 2017,
Accepted 15 Sep 2017

Keywords

- ✓ Synthesis
- ✓ Carbon steel;
- ✓ Hydrochloric acid;
- ✓ EHTC
- ✓ Corrosion inhibition;
- ✓ Electrochemical techniques
- ✓ DFT

H. Oudda

ouddahassan@gmail.com
+212698192251

Abstract

The new derivative of 1, 2,3-triazole in basic 8-hydroxyquinoline namely ethyl 4-amino-1-((8-hydroxyquinolin-5-yl)methyl)-1H-1,2,3-triazole-5-carboxylate (EHTC) was synthesized and characterized by NMR spectroscopic. This compound was tested as corrosion inhibitor for carbon steel in a 1.0 M HCl solution using Gravimetric, potentiodynamic polarization curves and electrochemical impedance spectroscopy. Potentiodynamic polarization curves measurements showed that the investigated compound acts as mixte-type inhibitor. Its inhibition efficiency improved with concentration and reached a maximum 91 % at 10^{-3} M. In addition, the temperature effect on the in the inhibition efficiency of EHTC was also studied in the temperature range of 298–328 K. It is found that the inhibition efficiency decreases with temperature. Indeed, the adsorption of the studied inhibitor on the mild steel was well described by the Langmuir isotherm and the calculated ΔG_{ads}^* value showed that corrosion inhibition was controlled by a chemisorptions process. Quantum chemical calculations were used to correlate the inhibition ability of EHTC with its electronic structural parameters.

1. Introduction

The acid solutions are widely used in many industrial applications such as pickling, cleaning, elimination of located deposits and numerous processes of industrial synthesis. Due to their aggressiveness, the use of the corrosion inhibitors became essential to limit this attack of the metallic materials [1]. This use must be estimated according to the particular parameters of the system, the type of the acid, its concentration, temperature solution, presence of dissolved organic or inorganic substances and especially on the type of metallic materials.

In general, for each material there exists a family of inhibitors favorable to a satisfactory protection against corrosion. Organic compounds containing unsaturated bonds and/or heteroatom's such as O, N and S, are often acted as the best corrosion inhibitors in acid medium [2-8].

The families quinoline have been widely used as a corrosion inhibitor, by way of example Ganesha Achary and al., have studied the corrosion inhibition of ordinary steel in 1 M HCl by 3-formyl-8-hydroxyquinoline and they founded that its inhibition efficiency reaches 92 % [9]. In addition, El Faydy and al. have tested the corrosion

inhibition effect of 5-chloromethyl-8-hydroxyquinoline on mild steel corrosion in the same media and they found that the inhibition efficiency reaches 91 % [10]. On the other hand Lgaz and al. were found that the corrosion inhibition of 5,5'-((2-hydroxypropane-1,3-diyl)bis(oxy))bis(methylene))bis-(8-quinolinol) for mild steel in 1 M HCl reaches 92 % [11]. In our recent work, 5-((4-phenyl-4,5-dihydro-1H-tetrazol-1-yl)methyl)quinolin-8-ol reached more than 91% in HCl solution [12].

In this work, we have studied the effect of novel triazole derivative based on 8-hydroxyquinoline, namely ethyl 5-amino-1-((8-hydroxyquinolin-5-yl)methyl)-1H-1,2,3-triazole-4-carboxylate (EHTC) for carbon steel in 1.0 M HCl using electrochemical measurements. And then, Quantum chemical calculations have been performed using DFT, and several quantum chemical indices are calculated and correlated with the inhibitive effect of inhibitor.

2. Experimental details

2.1. Materials

The steel used in this study is a carbon steel (XC38) which its chemical composition is given in Table 1.

Table1: Chemical Composition of Carbon-Steel.

Elements	Fe	C	Si	Mn	Cu	S	Cr	Co	Ti	Ni
Wt. %	Rest	0.37	0.23	0.68	0.16	0.016	0.077	0.09	0.011	0.059

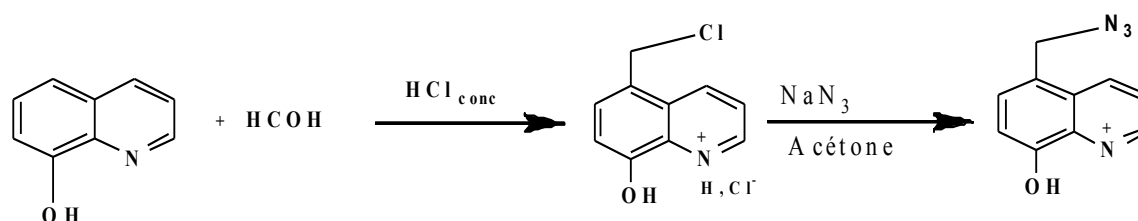
2.2. Solutions

The corrosive solution is a 1.0 M HCl, obtained by dilution with distilled water of a commercial acid concentrated in 37 %. The concentration range of the tested inhibitor was from 10^{-6} M to 10^{-3} M

2.3. Synthesis

a- synthesis of 5-azidomethyl-8-hydroxyquinoline

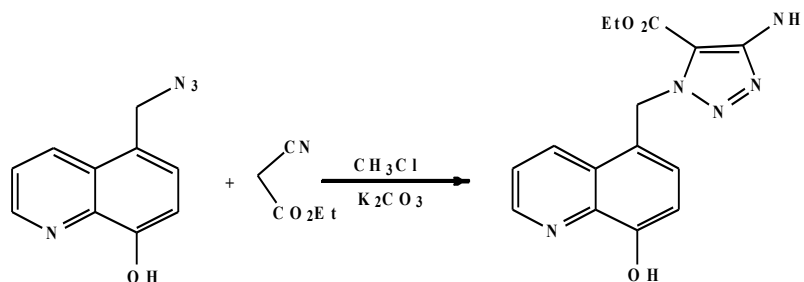
The synthesis of 5-azidomethyl-8-hydroxyquinoline was prepared according to method brought back in the literature [13].



Scheme 1: Preparation of 5-azidomethyl-8-hydroxyquinoline

b- Synthesis of ethyl 5-amino-1-((8-hydroxyquinolin-5-yl)methyl)-1H-1,2,3-triazole-4-carboxylate

To a stirred solution of 5-azidomethyl-8-hydroxyquinoline (1.4×10^{-3} mol) and ethyl 2 cyanoacetate (1.8×10^{-3} mol). The resulting mixture was heated at 80 °C for 24 h. The reaction was monitored by thin layer chromatography (TLC). After completion and cooling to room temperature, water (50 mL) was subsequently added and the product extracted with methylene chloride (DCM) (3×80 mL). The combined organic phases were combined, dried over anhydrous sodium sulfate, filtered and the solvent was removed by rotary evaporation. The crude product was purified by column chromatography with hexane/acetone (7:3) to furnish the desired product.



Scheme 2: Preparation of ethyl 5-amino-1-((8-hydroxyquinolin-5-yl)methyl)-1H-1,2,3-triazole-4-carboxylate

The compound was characterized by ^1H NMR and ^{13}C NMR. ^1H NMR (300 MHz, DMSO- d_6), $\delta\text{ppm} = 0.774$ (t, 3 H, CH_3), 1.121 (q, 2 H, CH_2), 7.035-8.850 (m, 5 H, quinoline), 3.927 (s, 2 H, quinoline - CH_2 -triazole), 9.842 (s, 2 H, NH_2), 3.40 (s, H of trace H_2O present in DMSO- d_6).

^{13}C NMR (300 MHz, DMSO- d_6), $\delta\text{ppm} = 13.852$ (CH_3 - CH_2 - $\text{C}=\text{O}$), 62.839 (CH_3 - CH_2 - $\text{C}=\text{O}$), 53.868 (quinoline- CH_2 -), 111.024-153.527 (CH , C quinoline and triazole), 168.689 (CH_3 - CH_2 - $\text{C}=\text{O}$).

^1H NMR spectra (300 MHz, DMSO- d_6) ^{13}C NMR spectra (300 MHz, DMSO- d_6)

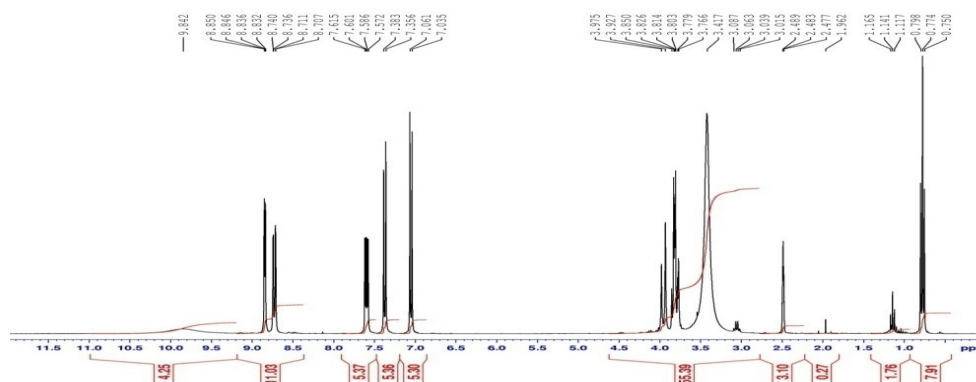


Figure 1: ^1H NMR spectrum of ethyl 4-amino-1-((8-hydroxyquinolin-5-yl)methyl)-1H-1,2,3-triazole-5-carboxylate

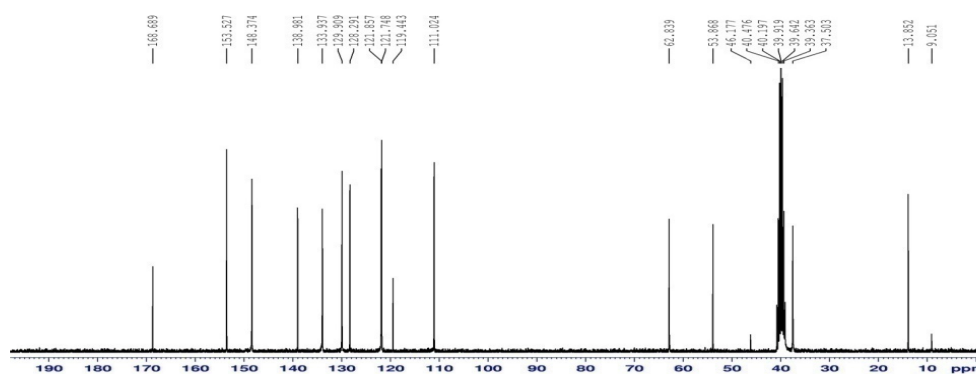


Figure 2: ^{13}C NMR spectrum of ethyl 4-amino-1-((8-hydroxyquinolin-5-yl)methyl)-1H-1,2,3-triazole-5-carboxylate

2.4. Corrosion tests

2.4.1 Gravimetric Study

Gravimetric experiments were performed according to the standard methods [14], the carbon steel specimens were abraded with a series of emery papers SiC (120, 600, and 1200 grades) and then washed with distilled water and acetone. After weighing accurately, the specimens were immersed in a 60 mL of 1.0 M HCl solution with and without addition of different concentrations of inhibitor EHTC.

All the aggressive acid solutions were open to air. After 6 hours of immersion, the specimens were taken out, washed, dried, and reweighed accurately. In order to get good reproducibility, all measurements were performed few times and average values were reported. Thus, the inhibition efficiency (η_w) was calculated as follows:

$$\eta_w = \frac{\omega_{corr}^0 - \omega_{corr}}{\omega_{corr}^0} \times 100 \quad (1)$$

Where ω_{corr}^0 and ω_{corr} are the corrosion rate values without and with inhibitor, respectively.

2.4.2. Electrochemical measurements

The electrochemical measurements were carried out using Volta lab (Tacussel- Radiometer PGZ 100) potentiostat and controlled by Tacussel corrosion analysis software model (Voltmaster 4) at under static condition. The corrosion cell used had three electrodes; the reference electrode was a saturated calomel electrode (SCE), the platinum electrode was used as auxiliary electrode of surface area of 1 cm^2 and the working electrode was carbon steel. All potentials given in this study were referred to this reference electrode. The working electrode was immersed in test solution for 30 min to a establish steady state open circuit potential (Eocp). After measuring the Eocp, the electrochemical measurements were performed. All electrochemical tests have been performed in aerated solutions at 298 K. The EIS experiments were conducted in the frequency range with high limit of 100 kHz and different low limit 0.01 Hz at open circuit potential, with 10 points per decade, at

the rest potential, after 30 min of acid immersion, by applying 10 mV ac voltage peak-to-peak. Nyquist plots were made from these experiments.

After AC impedance test, the potentiodynamic polarization measurements of carbon steel substrate in inhibited and uninhibited solution were scanned from cathodic to the anodic direction between -600mV to -200 mV, with a scan rate of 1 mV s⁻¹. The potentiodynamic data were analysed using the polarization VoltaMaster 4 software. The linear Tafel segments of anodic and cathodic curves were extrapolated to corrosion potential to obtain corrosion current densities (*i*_{corr}). From the polarization curves obtained, the corrosion current (*i*_{corr}) was calculated by curve fitting using the equation:

$$i = i_a + i_c = i_{\text{corr}} \left\{ \exp \left[b_a \times (E - E_{\text{corr}}) \right] - \exp \left[b_c \times (E - E_{\text{corr}}) \right] \right\} \quad (2)$$

where *i*_{corr} is the corrosion current density (A cm⁻²), *b*_a and *b*_c are the Tafel constants of anodic and cathodic reactions (V⁻¹), respectively. These constants are linked to the Tafel slopes β (V/dec) in usual logarithmic scale given by equation (3):

$$\beta = \frac{\ln 10}{b} = \frac{2.303}{b} \quad (3)$$

The inhibition efficiency was evaluated from the measured *i*_{corr} values using the following relationship:

$$\eta_{\text{pp}} = \frac{i_{\text{corr}}^0 - i_{\text{corr}}}{i_{\text{corr}}^0} \times 100 \quad (4)$$

where *i*_{corr}⁰ and *i*_{corr} are the corrosion current densities for steel electrode in the uninhibited and inhibited solutions, respectively.

2.4.3. Computational procedures

The quantum chemical calculations were carried out to elucidate the correlation between the inhibitor molecular structure and its efficiency. Quantum chemical calculations were performed using density functional theory (DFT) with the Beck's three parameter exchange functional along with the Lee-Yang-Parr non local correlation functional (B3LYP) with 6-31G (d, p) basis set implemented in Gaussian 09 program package [15,16]. This approach is widely utilized in the analysis of the characteristics of corrosion process.

The following quantum descriptors were calculated from the obtained optimized structure: energy of highest occupied molecular orbital (*E*_{HOMO}), energy of lower unoccupied molecular orbital (*E*_{LUMO}), electronegativity (*χ*), the global hardness (*η*), global softness (*σ*), electron affinity (*A*), ionization potential (*Pi*), the total molecular dipole moment (*μ*) and the total energy (TE) have been calculated [17-22].

$$\eta = \frac{\Delta E}{2} = \frac{E_{\text{LUMO}} - E_{\text{HOMO}}}{2} \quad (5)$$

$$\sigma = \frac{1}{\eta} = -\frac{2}{E_{\text{HOMO}} - E_{\text{LUMO}}} \quad (6)$$

$$Pi = -E_{\text{HOMO}} \quad (7)$$

$$A = -E_{\text{LUMO}} \quad (8)$$

$$\chi = -Pi \quad (9)$$

The number of transferring electrons (*ΔN*) was calculated according to the method of the quantum chemical:

$$\Delta N = \frac{\chi_{\text{Fe}} - \chi_{\text{inh}}}{2(\eta_{\text{Fe}} + \eta_{\text{inh}})} \quad (10)$$

where *χ*_{Fe} and *χ*_{inh} represent the absolute electronegativity of iron and the inhibitor molecule, *η*_{Fe} and *η*_{inh} denote respectively the absolute hardness of iron and the inhibitor molecule. Theoretically *χ*_{Fe} = 7.0 eV and *η*_{Fe} = 0 for the calculation of the number of transferring electrons.

Using left and right derivatives with respect to the number of electrons, electrophilic and nucleophilic Fukui functions for a site *k* in a molecule can be defined [23].

$$f_k^+ = P_k(N+1) - P_k(N) \quad (\text{For nucleophilic attack}) \quad (11)$$

$$f_k^- = P_k(N) - P_k(N-1) \quad (\text{For electrophilic attack}) \quad (12)$$

*P*_k(*N*), *P*_k(*N*+1) and *P*_k(*N*-1) are the natural populations for the atom *k* in the neutral, anionic and cationic species respectively

3. Electrochemical measurement

3.1. Potentiodynamic polarization curves

Figure 3 represents the potentiodynamic polarization curves for carbon steel in 1.0 M HCl at room temperature, in the absence and presence of different concentration of EHTC. Their corresponding electrochemical parameters such as corrosion potential (E_{corr}), cathodic Tafel slopes (β_c) and corrosion current density (i_{corr}) are presented in Table 2. It is noted that the addition of EHTC pulls an important decrease of current densities for all concentrations with a slight shift in the corrosion potential (E_{corr}). In addition, it is noted that both anodic and cathodic currents decrease with EHTC concentration indicating that the EHTC reduces anodic dissolution and also retards the hydrogen evolution reaction.

As well, Table 2 indicated that the addition of EHTC leads to increase the inhibition efficiency with concentration to reach 92 % at 10^{-3} M. this can be explained by the inhibitor molecules adsorption on the metallic surface.

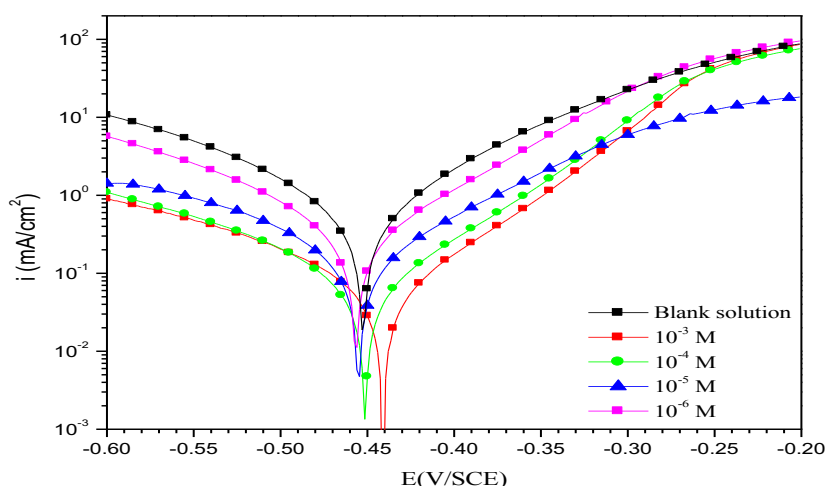


Figure 3: Potentiodynamic polarization curves for carbon steel in 1.0 M HCl containing different concentrations of EHTC.

Table 2: Electrochemical parameters and inhibition efficiencies values of carbon steel in 1.0 M HCl containing different concentrations of ETHC at 298 K.

	C_{inh} (M)	$-E_{\text{corr}}$ (mV/SCE)	$-\beta_c$ (mV dec ⁻¹)	i_{corr} ($\mu\text{A cm}^{-2}$)	η_{pp} (%)
Blank solution	00	454.4	101.1	590.8	--
EHTC	10-3	443.6	88.1	45.9	92
	10-4	453.3	84.5	54.5	91
	10-5	457.5	103.3	137.4	77
	10-6	459.1	77.2	224	62

3.2 Electrochemical impedance spectroscopic studies

The behavior of corrosion inhibition of the carbon steel in 1.0 M HCl solution without and with different concentrations of EHTC after immersion for 30 minutes at 298 K at E_{OCP} was studied by electrochemical impedance spectroscopy (EIS). The obtained results are presented in Figure 4. It is noted that the diagrams are in the form of semicircles which their sizes increase with inhibitor concentration, indicating a process of charge transfer is marked well and that the protection is improved in the presence of EHTC. Thus, the inhibition efficiencies, η_{EIS} , were calculated from the R_{ct} values at different concentrations using the following equation [24]:

$$\eta_{\text{EIS}} = \frac{R_{\text{ct}} - R_{\text{ct}}^0}{R_{\text{ct}}} \times 100 \quad (13)$$

where R_{ct}^0 and R_{ct} are the charge transfer resistance values in the absence and presence of inhibitor, respectively. All electrochemical parameters which extracted using the electrical equivalent circuits (Figure 5) are presented in Table 3. It is noted that the transfer resistance, R_{ct} , increases with inhibitor concentrations to reach a

maximum at 10^{-3} M of EHTC. This evolution is most probably due to the travel of water molecules by the Cl^- ions of the acid and the adsorption of the organic molecules on the metallic surface.

However, the double layer capacitance decreases with EHTC concentrations. This decrease can be interpreted by a decrease in the active surface of the metal which is due to the adsorption of EHTC molecules on carbon steel surface and leads to an increase in the inhibition efficiency. The expression of the double layer capacity presented in the Helmutz model by [25]:

$$C_{dl} = \frac{\epsilon_0 \times \epsilon}{d} \times S \quad (14)$$

where d is the thickness of the double layer, S is the surface area of the electrode, ϵ_0 is the permittivity of vacuum (8.85×10^{-14} F/cm) and ϵ is the local dielectric constant. This data suggests that the inhibitor acts by adsorption at the metal solution/interface [26]. In the other hand, it is remarked that the inhibition efficiency increases with inhibitor concentration to attain a maximum value of 90 % at 10^{-3} M of EHTC.

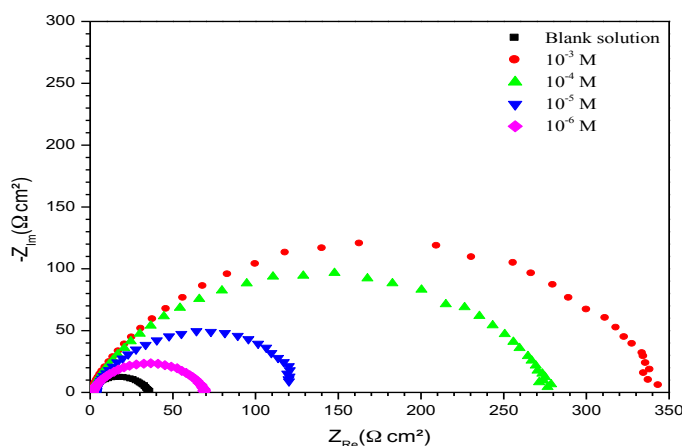


Figure 4: Nyquist plots for carbon steel in 1.0 M HCl in the absence and presence of various concentrations of EHTC at

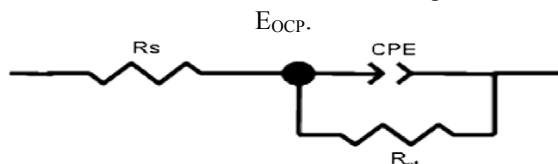


Figure 5: Electrical equivalent circuit used for modeling the metal/solution interface.

Table 3: Electrochemical data of EIS for carbon steel in 1.0 M HCl in the absence and presence of different concentrations of EHTC.

	C_{inh} (M)	R_{ct} ($\Omega \text{ cm}^2$)	C_{dl} ($\mu\text{F}/\text{cm}^2$)	η_{EIS} (%)
Blank solution	00	34.85	114.1	-
EHTC	10^{-3}	343.6	46.31	90
	10^{-4}	278.0	57.23	87
	10^{-5}	110.8	90.72	68
	10^{-6}	69.60	106.0	50

3.3. Weight loss measurements

The weight loss of carbon steel corrosion in 1.0 M HCl in the absence and the presence of different concentrations of EHTC were determined after 6 h of immersion at 298 K. The obtained results are presented in Table 4. It is obvious from the Table 4 that the EHTC inhibits the carbon steel corrosion in 1.0 M HCl solution at all concentrations and the corrosion rate (W_{corr}) was decreased with increasing concentration to reach a maximum of 86 % at 10^{-3} M. So, the inhibition efficiency of EHTC can be explained in terms of adsorption on the metal surface. However, the corrosion inhibition of metals using organic compounds was explained by their adsorption on the metallic surface. The latter is under three much known forms. The phenomenon of adsorption can be implemented by the study of the isotherms of adsorption.

Table 4: Weight loss data of carbon steel in 1.0 M HCl without and with different concentrations of EHTC at 298 K after 6 h of immersion.

	C_{inh} (M)	W_{corr} ($mg\ cm^{-2}\ h^{-1}$)	η_w (%)
HCl	00	0.4292	--
EHTC	10^{-3}	0.0583	86
	10^{-4}	0.0625	85
	10^{-5}	0.1183	72
	10^{-6}	0.1893	55

In order to study the variation of the quantity adsorbed according to the inhibitor concentration, it is supposed that the EHTC adsorption follows the Langmuir isotherm which the coverage ratio of the metal surface is given by:

$$\theta = \frac{K_{ads} C_{inh}}{K_{ads} C_{inh} + 1} \quad (15)$$

By rearranging this equation:

$$\frac{C_{inh}}{\theta} = \frac{1}{K_{ads}} + C_{inh} \quad (16)$$

where K_{ads} is the adsorption equilibrium constant, C_{inh} is the inhibitor concentration, and θ is the surface coverage. Figure 6 shows the plots of C_{inh}/θ versus C_{inh} . It is found that the slope and the coefficient correlation are reported almost unity suggesting that the Langmuir adsorption isotherm model provides the best description of the adsorption behavior.

In addition, the K_{ads} values can be calculated from the intercept lines on the C_{inh}/θ . This is related to the free energy of adsorption (ΔG_{ads}^*) with the following equation [27,28]:

$$K_{ads} = \frac{1}{55.55} \exp\left(\frac{-\Delta G_{ads}^*}{RT}\right) \quad (17)$$

where 55.55 value represents the water concentration in solution ($mol\ L^{-1}$), R is the universal gas constant and T is the absolute temperature.

The free energy of adsorption, ΔG_{ads}^* can be calculated. It is well known that ΔG_{ads}^* values on the order of -20 $kJ\ mol^{-1}$ or less indicate a physisorption, while those more negative than -40 $kJ\ mol^{-1}$ involve charge sharing or transfer from the inhibitor molecules to the metal surface to form a coordinate chemical bond (chemisorptions), while values between -20 $kJ\ mol^{-1}$ and -40 $kJ\ mol^{-1}$ indicate both physisorption and chemisorption [29]. In our case, ΔG_{ads}^* value is -43.80 $kJ\ mol^{-1}$. This value indicated that adsorption of EHTC occurs via both chemisorption [30].

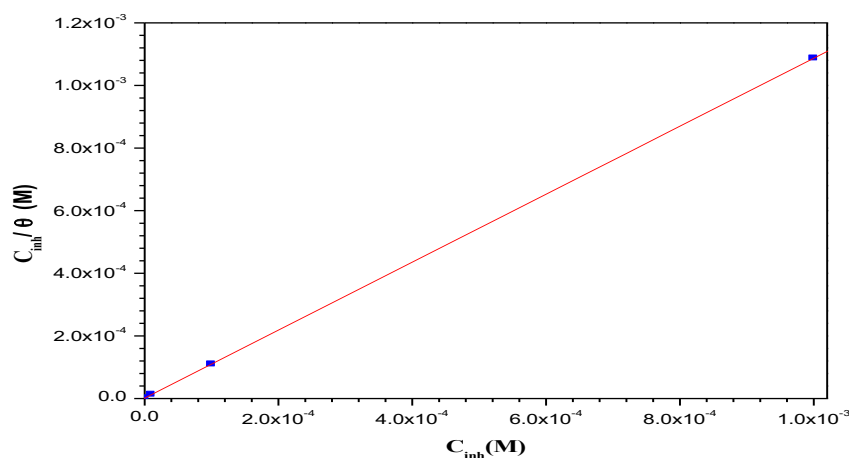


Figure 6: Langmuir adsorption isotherm plot for carbon steel in 1.0 M HCl at different concentrations of EHTC.

3.4. Effect of temperature

The temperature is one of the factors which can modify the behavior of materials in corrosive medium given as well as the inhibitive efficiency of compound. So, when the temperature increases a change on the inhibitors actions appear. Given the importance of this factor, we carried out tests for the plotting of the potentiodynamic polarization curves of carbon steel 1.0 M HCl without and with 10^{-3} M of EHTC at different temperature range from 298 K to 328 K and the obtained results are shown in Figures 7 and 8. Their electrochemical parameters values are summarized in Table 5. It is noted that the corrosion rate increases with temperature for both cases in the absence and presence of EHTC. It is noted also that the inhibition efficiency decreases with temperature, and by way of example, it is decreases until 85 % in 328 K at 10^{-3} M.

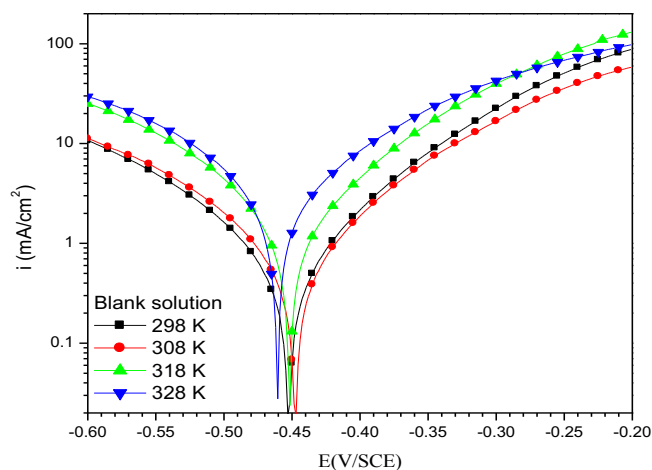


Figure 7: Potentiodynamic polarization curves for carbon steel in 1.0 M HCl at different temperatures.

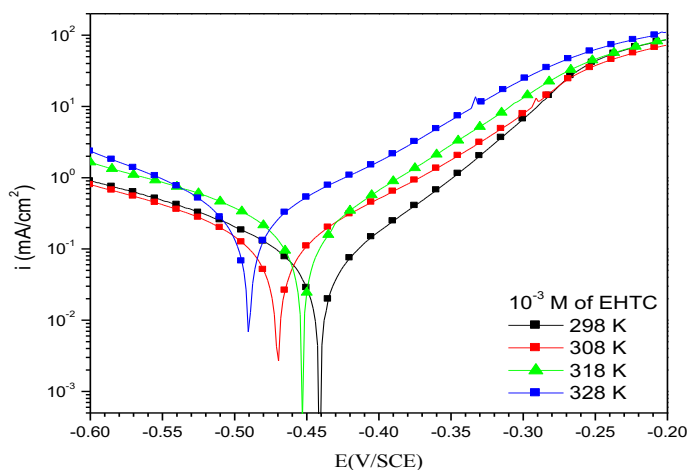


Figure 8: Potentiodynamic polarization curves for carbon steel in 1.0 M HCl in the presence of 10^{-3} M of EHTC at different temperatures

Table 5: Electrochemical parameters of carbon steel in 1.0 M HCl in the absence and presence of 10^{-3} M of EHTC at different temperatures.

	T (K)	$-E_{corr}$ (mV/SCE)	i_{corr} ($\mu\text{A cm}^{-2}$)	$-\beta_c$ (mV dec $^{-1}$)	η_{PP} (%)
Blank solution	298	454.4	590.8	101.1	-
	308	451.1	666.8	104.9	-
	318	454.8	982.4	111.1	-
	328	464.3	2368.5	101	-
10^{-3} M of EHTC	298	443.6	45.9	88.1	92
	308	472.6	95.06	119.1	86
	318	455.5	147.3	114.7	85
	328	493.4	337.2	130.2	85

In addition, in the absence of inhibitor, it is found that the cathodic Tafel slopes stay almost constant indicating no change in the hydrogen reduction; while in the presence of EHTC a change in this mechanism with increasing of temperature.

The Arrhenius dependence observed between the corrosion current and the temperature can be determined according to the relation:

$$i_{corr} = A \exp\left(-\frac{E_a}{RT}\right) \quad (18)$$

where i_{corr} is the corrosion current density, A is the Arrhenius preexponential factor, E_a is the apparent activation energy, R is the universal gas constant and T is the absolute temperature.

However, kinetic parameters such as enthalpy and entropy of corrosion process may be evaluated from the temperature effect. An alternative formulation of Arrhenius equation is [31,32]:

$$i_{corr} = \frac{RT}{Nh} \exp\left(\frac{\Delta S_a}{R}\right) \exp\left(-\frac{\Delta H_a}{RT}\right) \quad (19)$$

where h is plank's constant, N is Avogadro's number, ΔS_a and ΔH_a are the entropy and enthalpy of activation, respectively. The apparent activation energy was determined from the slopes of $\ln i_{corr}$ vs $1/T$ graph depicted in Figure 9. The straight lines are obtained with a slope $(-\Delta H_a/R)$ and intercept $(\ln R/Nh + \Delta S_a/R)$ from which these parameters can be calculated (Figure 10).

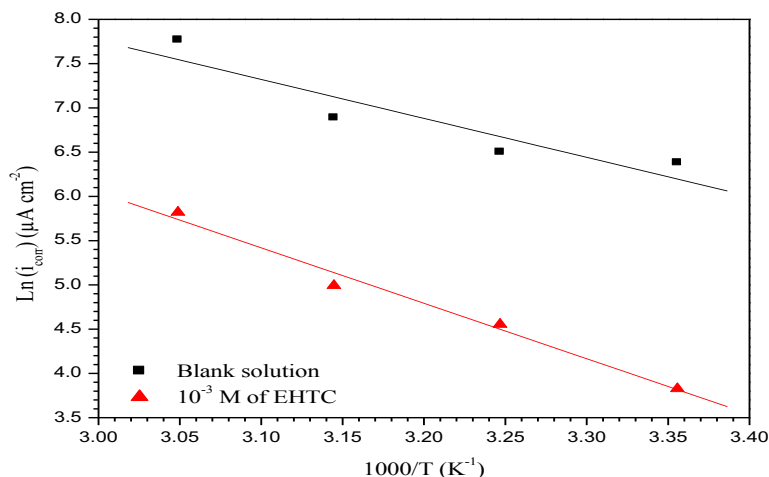


Figure 9: Arrhenius plots for carbon steel in 1.0 M HCl in the absence and presence of 10^{-3} M of EHTC at different temperatures.

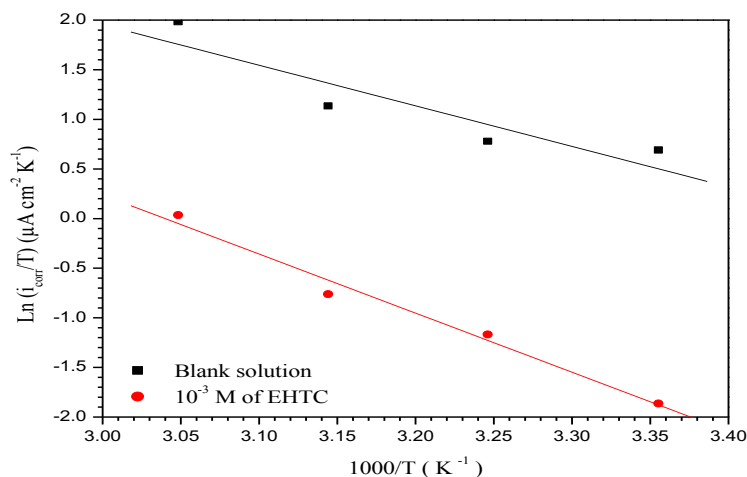


Figure 10: Transition-state plots for carbon steel in 1.0 M HCl in the absence and presence of 10^{-3} M of EHTC at different temperatures.

It is noted that the activation energy E_a value increases from 36.5 kJ mol^{-1} to $52.01 \text{ kJ mol}^{-1}$ with inhibitor addition. This behavior is related to the phenomenon of physisorption of inhibitor molecules on metallic surface [33,34]. It is remarked also that the ΔH_a value increases from $33.98 \text{ kJ mol}^{-1}$ to $49.50 \text{ kJ mol}^{-1}$. The positive sign of these enthalpies reflects the endothermic nature of the dissolution carbon steel process which its dissolution becomes difficult. We note that the ΔS_a value increases negatively from $-79 \text{ J mol}^{-1} \text{ K}^{-1}$ to $-47 \text{ J mol}^{-1} \text{ K}^{-1}$. This result interpreted as an increase in disorder [35].

3.5. Quantum chemical calculations

The Frontier Orbital's Molecular (HOMO and LUMO) are very important for describing chemical reactivity. The HOMO containing electrons, represents the ability (E_{HOMO}) to donate an electron, whereas, LUMO haven't electrons, as an electron acceptor represents the ability (E_{LUMO}) to obtain an electron. The energy gap between

these orbitals determined by optimization. The quantum chemical parameters were calculated according [36,37] and presented in Table 6 and the optimized molecule structure (EHTC) is depicted in Figure 11.

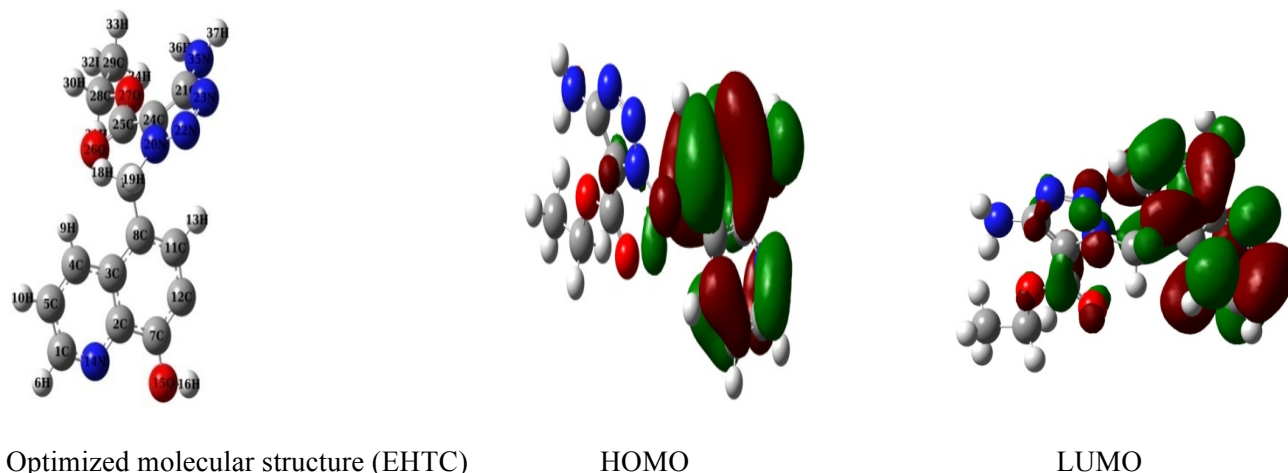


Figure 11: Optimized molecular structures, HOMO and LUMO of EHTC.

The Mulliken charge distribution with dipole moment vector (μ), the contour and the surface representation of the electrostatic potential are presented in Figure 12.

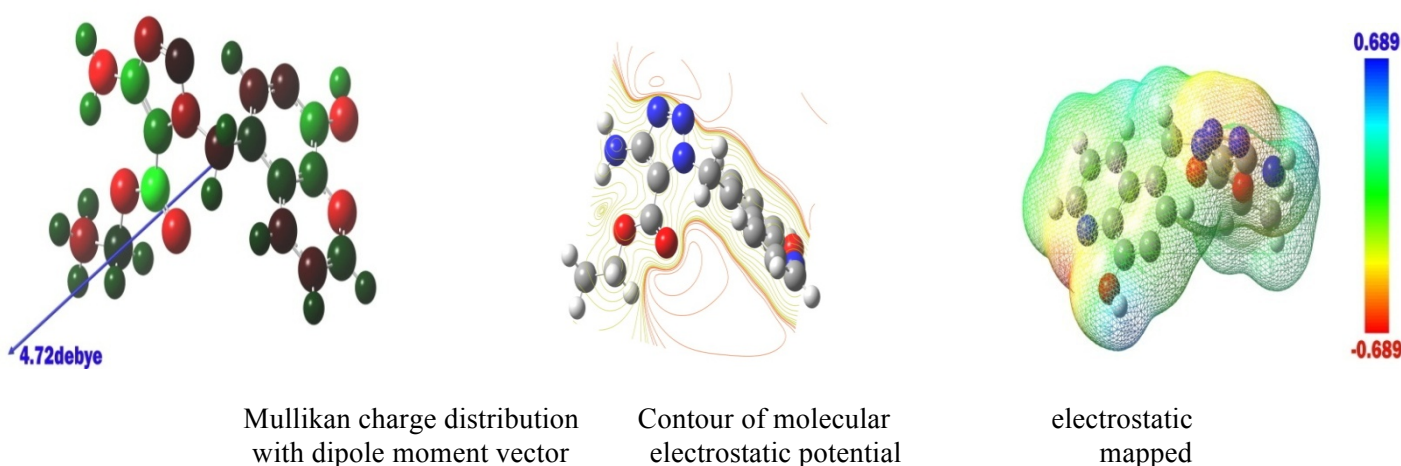


Figure 12: Mulliken charges with dipole moment and electrostatic properties of EHTC.

However, the electrostatic potential values were presented using different colors such as blue, yellow, green and red. The red colors represent the negative parts around the oxygen and nitrogen atoms of EHTC (electrophilic active regions), the blue colors represent the positive parts around the C-H group (the nucleophilic regions) and the green color represents the zero electrostatic potential regions [38]. Thus, it is noted that the nitrogen, oxygen atoms and some carbon atoms of the studied inhibitor hold negative charges, and then these atoms can be responsible for a nucleophilic attack towards the carbon steel surface. This remark will be confronted here after with the indices of Fukui.

Table 6: Molecular properties of EHTC obtained from the optimized structure using DFT at the B3LYP/6-31G

Parameters	E_{LUMO} (eV)	E_{HOMO} (eV)	ΔE (eV)	μ (debyes)	η (eV)	σ ($e V^{-1}$)	Pi (eV)	χ (eV)	A (eV)	ΔN (eV)	TE (u a)
EHTC	-2.640	-5.687	3.047	4.726	1.523	0.656	5.687	4.163	2.640	0.931	-1079.37

It is observed from this Table, that the EHTC has a relatively higher energy of HOMO, this means a better inhibitory activity with increasing adsorption of the inhibitor on metallic surface and lower energy of LUMO, which can be in favor of bonding with metal surface. In addition, as a result of high values of HOMO, EHTC

has a tendency to donate electrons to those acceptor molecules with empty molecular orbital. The ground-state electronic configuration of Fe atom is $1s^2 2s^2 2p^6 3s^2 3p^6 4s^2 3d^6$. The incompletely occupied 3p orbital of Fe could bond with HOMO of EHTC, while the filled 3s orbital, it could interact with LUMO of EHTC.

However, the χ , η , σ and ΔN values are also listed in Table 6. According to some studies [39], the parameter of χ is related to the chemical potential, and higher value of χ means better inhibitive performance. On the other hand, η is equal to $\Delta E/2$, and the lower η implies more polarizability and higher inhibition efficiency. The parameter of σ is reciprocal to η , thus high value of σ is related to more efficiency. Values of ΔN exhibit inhibitive performance resulted from electrons donations. If $\Delta N < 3.6$, the inhibition efficiency increases with the increase in electron-donation ability to the metal surface.

The reactive regions in a molecule can be analyzed using Fukui indices. These represent the regions in a molecule susceptible for electrophilic and nucleophilic attack. Fukui functions can be evaluated using Mulliken population analysis of atoms in a molecule depending on the direction of electron transfer [40].

Generally, the high value of f_K^- is the preferred site for nucleophilic attack, while the sites with a high value of f_K^+ are preferred for electrophilic attack [34]. These Fukui indices for the tested EHTC were presented in Table 7. In EHTC atoms C3 (0.004), C17 (0.017), C24 (0.025) and C25 (0.011) presented the highest values of f_K^- regarding the most susceptible sites for nucleophilic attacks. In addition, the C7 (0.037), C11 (0.066), N20 (0.042), C21 (0.031), C28 (0.019) and C21 (0.028) is the preferable sites for electrophilic attacks and consequently donating charges to the carbon steel surface, as they presented the highest values of f_K^+ . Based on these findings, the distribution of the active sites is quite different. This implies the highest capacity of adsorption of EHTC on the carbon steel surface confirming the high obtained experimental inhibition efficiency.

Table 7. Values of the Fukui function considering Natural Population analysis (NPA) of EHTC molecule calculated at the B3LYP / 6-31 G (d, p).

Atomes	P(N)	P (N+1)	P (N-1)	f_k^+	f_k^-
C1	5.975	5.932	6.006	-0.043	-0.031
C2	5.861	5.830	5.864	-0.031	-0.003
C3	6.076	6.080	6.094	0.004	-0.018
C4	6.191	6.157	6.201	-0.034	-0.01
C5	6.269	6.241	6.323	-0.028	-0.054
C7	5.778	5.720	5.741	-0.058	0.037
C8	6.035	5.977	6.101	-0.058	-0.066
C11	6.312	6.298	6.246	-0.014	0.066
C12	5.885	5.782	6.419	-0.103	-0.534
N14	7.413	7.369	7.444	-0.044	-0.031
O15	8.684	8.602	8.710	-0.082	-0.026
C17	6.273	6.290	6.274	0.017	-0.001
N20	7.177	7.145	7.135	-0.032	0.042
C21	5.701	5.644	5.670	-0.057	0.031
N22	7.053	7.006	7.045	-0.047	0.008
N23	7.280	7.252	7.339	-0.028	-0.059
C24	5.996	6.021	6.065	0.025	-0.069
C25	5.202	5.213	5.221	0.011	-0.019
O26	8.607	8.588	8.609	-0.019	-0.002
O27	8.520	8.567	8.584	0.047	-0.064
C28	6.135	6.120	6.116	-0.015	0.019
C30	6.715	6.718	6.709	0.003	0.006
N35	7.891	7.768	7.863	-0.123	0.028

Conclusion

In this study, corrosion inhibition efficiency of ethyl 5-amino-1-((8-hydroxyquinolin-5-yl)methyl)-1H-1,2,3-triazole-4-carboxylate (EHTC) on carbon steel in 1.0 M HCl was investigated by electrochemical measurements coupled with Quantum chemical calculations. It is found that the EHTC shows a good inhibition performance for carbon steel in 1.0 M HCl solution and its inhibition efficiency increases with concentrations and decreases with temperature. It is found that the EHTC acts as a mixed-typed inhibitor which suppresses both the anodic

and cathodic process by chemisorptions on the carbon steel surface, and its adsorption obeys Langmuir adsorption isotherm. Electrochemical impedance spectroscopy data reveals an increase in transfer resistance R_{ct} values, which accounted for good inhibition efficiency. Quantum chemical studies also support the experimental studies.

Acknowledgments-This work was supported by “Ibn Tofail University”, “CNRST” and the “Moroccan Ministry of Higher Education”. We are pleased to acknowledge them.

References

1. D. D. N. Singh, T. B. Singh, B. Gaur, *Corros. Sci.* 37(6) (1995) 1005.
2. M. Rbaa, M. Galai, M. EL Faydy, Y. El Kacimi, Ebn M. Touhami, A. Zarrouk, B. Lakhri, *J. Mater. Environ. Sci.* 8 (10) (2017) 3529-3549.
3. M. Elbakri, R. Tourir, M. Ebn Touhami, A. Zarrouk, Y. Aouine, M. Sfaira, M. Bouachrine, A. Alami, A. El Hallaoui, *Res. Chem. Intermed.* 39(6) (2013) 2417.
4. M. Belayachi, H. Serrar, H. Zarrok, A. El Assyry, A. Zarrouk, H. Oudda, S. Boukhris, B. Hammouti, E.E. Ebenso, A. Geunbour, *Int. J. Electrochem. Sci.* 10(4) (2015) 3010.
5. A. Zarrouk, H. Zarrok, R. Salghi, R. Tourir, B. Hammouti, N. Benchat, L.L. Afrine, H. Hannache, M. El Hezzat, M. Bouachrine, *J. Chem. Pharm. Res.* 5(12) (2013) 1482.
6. H. Tayebi, H. Bourazmi, B. Himmi, A. El Assyry, Y. Ramli, A. Zarrouk, A. Geunbour, B. Hammouti, *Der Pharm. Chem.* 6(5) (2014) 220.
7. H. Tayebi, H. Bourazmi, B. Himmi, A. El Assyry, Y. Ramli, A. Zarrouk, A. Geunbour, B. Hammouti, E.E. Ebenso, *Der Pharm. Lett.* 6(6) (2014) 20.
8. M. Larouj, H. Lgaz, H. Serrar, H. Zarrok, H. Bourazmi, A. Zarrouk, A. Elmidaoui, A. Guenbour, S. Boukhris, H. Oudda, *J. Mater. Environ. Sci.* 6(11) (2015) 3251.
9. G. Achary, H. P. Sachin, Y. A. Naik, T. V. Venkatesha, *Mater. Chem. Phys.* 107(1) (2008) 44.
10. M. El Faydy, M. Galai, A. El Assyry, A. Tazouti, R. Tourir, B. Lakhri, A. Zarrouk, *J. Mol. Liq.* 219 (2016) 396.
11. H. Lgaz, R. Salghi, M. Larouj, M. Elfaydy, S. Jodeh, Z. Rouifi, B. Lakhri, H. Oudda, *J. Mater. Environ. Sci.* 7 (2016) 4471.
12. H. About, M. El Faydy, Z. Rouifi, F. Benhiba, H. Ramsis, M. Boudalia, H. Zarrok, H. Oudda, R. Tourir, M. El M'Rabet, I. Warad, A. Guenbour, B. Lakhri, *J. Mater. Environ. Sci.* 9 (1) (2018) 345-357.
13. B. Himmi, B. Messnaoui, S. Kitane, A. Eddaif, A. Alaoui, A. Bouklouz, M. Soufiaoui, *Hydrometallurgy*, 93(1) (2008) 39.
14. A. L. Essaghoulani, H. Elmsellem, M. Ellouz, M. El Hafi, M. Boulhaoua, N. K. Sebbar, E. M. Essassi, M. Bouabdellaoui, A. Aouniti, B. Hammouti, *Der Pharm. Chem.* 8(2) (2016) 297.
15. Y. Feng, S. Chen, W. Guo, Y. Zhang, G. Liu, *J. Electroanal. Chem.* 602 (2007) 115.
16. gaussian 03, Revision C.01, M.J. Frisch, G.W. Trucks, H.B. Schlegel, G.E. Scuseria, M.A. Robb, J.R. Cheeseman, Jr. J.A. Montgomery, T. Vreven, K.N. Kudin, J.C. Burant, J.M. Millam, S.S. Iyengar, J. Tomasi, V. Barone, B. Mennucci, M. Cossi, G. Scalmani, N. Rega, G.A. Petersson, H. Nakatsuji, M. Hada, M. Ehara, K. Toyota, R. Fukuda, J. Hasegawa, M. Ishida, T. Nakajima, Y. Honda, O. Kitao, H. Nakai, M. Klene, X. Li, J.E. Knox, H.P. Hratchian, J.B. Cross, C. Adamo, J. Jaramillo, R. Gomperts, R.E. Stratmann, O. Yazyev, A.J. Austin, R. Cammi, C. Pomelli, J.W. Ochterski, P.Y. Ayala, K. Morokuma, G.A. Voth, P. Salvador, J.J. Dannenberg, V.G. Zakrzewski, S. Dapprich, A.D. Daniels, M.C. Strain, O. Farkas, D.K. Malick, A.D. Rabuck, K. Raghavachari, J.B. Foresman, J.V. Ortiz, Q. Cui, A.G. Baboul, S. Clifford, J. Cioslowski, B.B. Stefanov, G. Liu, A. Liashenko, P. Piskorz, I. Komaromi, R.L. Martin, D.J. Fox, T. Keith, M.A. Al-Laham, C.Y. Peng, A. Nanayakkara, M. Challacombe, P.M.W. Gill, B. Johnson, W. Chen, M.W. Wong, C. Gonzalez, J.A. Pople (2004) Gaussian, Inc, Wallingford. Gaussian 03, Revision E.01, Gaussian, Inc, Wallingford CT (2004).
17. S. K. Saha, A. Hens, A. Roy Chowdhury, A. K. Lohar, N. C. Murmu, P. Banerjee, *Trans.* 2 (2014) 489-503.
18. S. K. Saha, P. Ghosh, A. Hens, N. C. Murmu, P. Banerjee, *Physica E*, 66 (2015) 332.
19. L. Pauling, *The nature of the chemical bond and the structure of molecules and crystals: an introduction to modern structural chemistry* Cornell university press. 18 (1960).
20. R. G. Parr, R. G. Pearson, *J. Am. Chem. Soc.* 105(26) (1983) 7512.
21. P. Geerlings, F. De Proft, W. Langenaeker, *Chem. Rev.* 103(5), (2003) 1793.

22. M. M. Kabanda, L. C. Murulana, M. Ozcan, F. Karadag, I. Dehri, I. B. Obot, E. E. Ebenso, *Int. J. Electrochem. Sci.*, 7 (2012) 5035.
23. J. J. Fu, S. N. Li, Y. Wang, X. D. Liu, *J. Mater. Sci.* 46(10) (2011) 3550.
24. S. A. Abd El-Maksoud, H. H. Hassan, *Mater. Corros.* 58(5) (2007) 369.
25. A. Ghazoui, R. Saddik, N. Benchat, M. Guenbour, B. Hammouti, S. S. Al-Deyab, A. Zarrouk, *Int. J. Electrochem. Sci.*, 7 (2012) 7080.
26. M. Manssouri, Y. El Ouadi, M. Znini, J. Costa, A. Bouyanzer, J. M. Desjobert, L. Majidi, *J. Mater. Environ. Sci.* 6(3) (2015) 631.
27. G. Avci, *Colloids Surf. A Physicochem. Eng. Asp.* 317(1) (2008) 730.
28. F. Xu, J. Duan, S. Zhang, B. Hou, *Mater. Lett.* 62(25) (2008) 4072.
29. M. Galai, M. Rbaa, Y. El Kacimi, M. Ouakki, N. Dkhirech, R. Tourir, B. Lakhriissi, M. Touhami, *Anal. Bioanal. Electrochem.*, 9(1) (2017) 80.
30. W. Li, Q. He, C. Pei, B. Hou, *Electrochim. Acta* 52 (2007) 6386.
31. M. Benabdellah, A. Tounsi, K. F. Khaled, B. Hammouti, *Arab. J. Chem.* 4(1) (2011) 17.
32. M. Dahmani, A. Et-Touhami, S. S. Al-Deyab, B. Hammouti, A. Bouyanzer, *Inter. J. Electrochem. Sci.* 5 (2010) 1060.
33. L. Bammou, M. Belkhaouda, R. Salghi, O. Benali, A. Zarrouk, S. S. Al-Deyab, I. Warad, H. Zarrok, B. Hammouti, *Int. J. Electrochem. Sci.* 9 (2014) 1506.
34. B. Hammouti, A. Zarrouk, S. S. Al-Deyab, I. Warad, *Orient. J. Chem.* 27 (2011) 23.
35. M. S. Morad, A. K. El-Dean, *Corros. Sci.* 48(11) (2006) 3398.
36. L. Herrag, B. Hammouti, S. Elkadiri, A. Aouniti, C. Jama, H. Vezin, F. Bentiss, *Corros. Sci.* 52 (2010) 3042.
37. S. Deng, X. Li, Xi. Xie, *Corros. Sci.* 80 (2014) 276.
38. T. Laabaissi, H. Lgaz, H. Oudda, F. Benhiba, H. Zarrok, A. Zarrouk, A. El Midaoui, B. Lakhriissi, R. Tourir, *J. Mater. Environ. Sci.* 8 (2017) 1054.
39. L.M. Rodriguez, W. Villamisr, L. Martinez, *Corros. Sci.* 48 (2006) 4053.
40. H. Mi, G. Xiao, X. Chen, *Comput. Theor. Chem.* 1072 (2015) 7.

(2018) ; <http://www.jmaterenvirosci.com>